Delaunay-Network Modelling of Creep Failure in Regular Polycrystalline Aggregates by Grain Boundary Cavitation

Burg, M.W.D. van der; Giessen, E. van der

Published in:
International Journal of Damage Mechanics

DOI:
10.1177/105678959400300202

Delaunay-Network Modelling of Creep Failure in Regular Polycrystalline Aggregates by Grain Boundary Cavitation

M. W. D. VAN DER BURG* AND E. VAN DER GIESSEN
Delft University of Technology
Lab. for Engineering Mechanics
P.O. Box 5033, 2600 GA Delft
The Netherlands

ABSTRACT: In polycrystalline materials at elevated temperatures subjected to stationary loading, creep fracture occurs as a result of failure mechanisms on the size scale of grains, namely the nucleation and diffusive growth of cavities until coalescence leads to microcracks. In this paper, a polycrystalline aggregate is modelled by so-called Delaunay elements associated with individual grain boundary facets, whose constitutive behaviour represents dislocation creep inside the grains as well as the cavitation processes on the associated grain facet. Free grain boundary sliding and the elastic deformation of the grain material are also taken into account. Unit cells of polycrystalline aggregates containing many grains are investigated, assuming regular hexagonal grains and allowing for cavitation on all facets, possibly at different rates. The development of creep damage is simulated numerically, starting from nearly no initial damage until an excessive number of microcracked grain boundaries cause disintegration of the polycrystal. It is demonstrated that continuous stress redistributions take place during the failure process, and that nonuniformities in the nucleation activity can cause the formation of "zones" of stress attenuation, where the grain boundaries damage and microcrack relatively quickly, separated by "shielded" regions. As a result of this, it is found that the orientation of the first microcracks is perpendicular to the macroscopic largest principal tensile stress, as expected, but that the orientation of the microcrack pattern is not necessarily in the same direction.

1. INTRODUCTION

THE PRACTICE OF engineering materials at elevated temperatures shows that, after years of stationary loading with low rates of deformation, so-called creep rupture may occur quite suddenly. It is observed that this failure mode is mostly intergranular, with the fracture surface showing a more or less uniform coverage of small dimples on the grain surfaces. These dimples are the remnants of cavities that have nucleated and grown on the grain boundaries (Cocks and Ashby, 1982).

1056-7895/94/02 0111-29 $6.00/0

Over the last few decades, investigations into the cause of creep rupture have been carried out experimentally as well as theoretically. It has been established that creep rupture is governed by three complex processes on a microscopic scale: 1) dislocation creep inside the grains, 2) nucleation and growth of cavities on the grain boundaries, and 3) grain boundary sliding. Driven by local creep and diffusion processes, grain boundary cavities grow until they are so large that neighbouring cavities coalesce and a microcrack is initiated. If enough grain boundaries have microcracked completely, they can link up with each other to cause macroscopic failure.

It is well-established now that the cavities grow by the diffusive motion of matter as well as by plastic creep flow (Needleman and Rice, 1980; Argon, 1982). At any given temperature, cavity growth by diffusion is dominant at relatively low stresses, whereas at high stresses the growth contribution by creep is most important. The first model that described the growth of a single cavity is due to Hull and Rimmer (1959). They assumed that cavities grow entirely by diffusion, and that the grains are rigid. Needleman and Rice (1980) pointed out that in certain circumstances, creep inside the grains interacts with the diffusional process so as to enhance the net void growth rate. Tvergaard (1984) gives analytical relations that capture their results and those of Sham and Needleman (1983) for a wide range of stress and temperature levels; these relationships will be the starting point for the considerations in the present study.

In the investigations mentioned above, the growth of a single cavity is studied under the assumption that the stresses "remote" relative to the cavity remain constant. It had been noted by Dyson (1976) however, that these stresses in the neighborhood of grain boundaries can deviate drastically from the applied, macroscopic stresses in situations where grain boundary diffusion is much faster than creep. But, in addition to this, it should be expected that these stresses do not remain constant in time on each facet in a polycrystal, even if the applied stress does remain constant. In practice, the grain boundary properties that govern cavity nucleation and/or growth will not be equal, leading to different rates of damage evolution on the participating grain boundaries. These variations in damage rates can cause continuous stress redistributions inside a polycrystalline aggregate during the process in order to ensure accommodation of the damage. In turn, these continuous stress redistributions should be expected to affect damage evolution, so that the process of damage accumulation in a polycrystalline aggregate is in general a spatially and temporally complex process which spans a range of length scales, from that of individual cavities up to the scale of a statistically large aggregate of grains.

The most recent advance in such a direction is work done by Van der Giessen and Tvergaard (1994a, 1994b), employing a multi-grain cell model analysis of a planar polycrystal model. In particular, they investigated the influence of the interaction between cavitating grain boundaries and the final linking up of micro-

cracked facets in polycrystalline aggregates with different initial grain boundary properties. Full field solutions are obtained numerically, but these analyses require a lot of computational time so that only cells with up to 30 grains are investigated. Along with confirming that the interactions are important, these studies also showed that the stress, and therefore the subsequent development of cavitation along a grain boundary, are quite uniform if cavity growth is dominated by diffusion and if stress-free grain boundary sliding can occur. In the present paper, we exploit this observation and, for those conditions, propose a more approximate approach to study creep failure in polycrystals through the nucleation and growth of cavities.

Following a brief recapitulation of the governing equations for creep and for the nucleation and growth of cavities, we will describe a representation of planar polycrystalline aggregates by means of so-called Delaunay elements. These elements are basically bar or truss elements, each of which represents an individual grain boundary and inhibits its state of damage. The elements are attributed special constitutive properties in order to account for cavitation, as well as for elastic deformations and creep in the adjacent grains, albeit in an approximate manner. This simple model allows for the simulation of the damage development in much larger polycrystal samples than feasible with the detailed model of Van der Giessen and Tvergaard (1994a, 1994b). The approach will be illustrated by unit cell analyses with cells containing several hundred grains. In those simulations, the polycrystal is assumed to comprise regular hexagonal grains, where cavitation can in principle occur on every grain boundary facet; however, cavitation on some facets can take place faster than on others. The ensuing nonuniform damage development in terms of cavity nucleation and growth until coalescence is simulated up to the point where a pattern of microcracks has developed that causes failure of the polycrystalline aggregate.

2. PROBLEM FORMULATION

The model to be presented is designed to apply to a polycrystalline metal subjected to temperatures in excess of about half the melting temperature. The creep strains are assumed to remain small, so that geometrical nonlinearities can be neglected. The assumption is usually adequate for typical operating conditions in high temperature components.

We consider a two-dimensional polycrystal model which is built up of regular hexagonal grains, similar to the model used by Van der Giessen and Tvergaard (1994a, 1994b). Imposing symmetries in the geometry as well as in the physical properties of the microstructure of the material, we can confine attention to a unit cell. The polycrystalline aggregate is taken to be subjected to macroscopic principal stresses Σ_1 and Σ_2 under plain strain conditions. The boundaries of the unit cell remain straight during the simulations in agreement with the symmetries imposed by the periodicity.

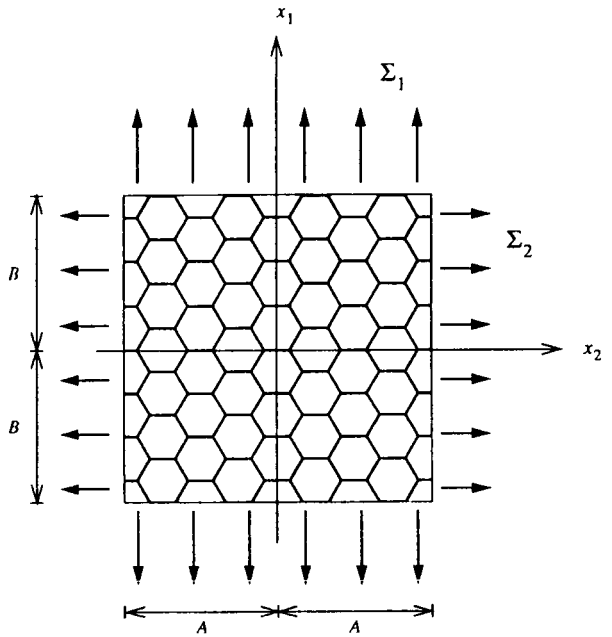

Figure 1. *The global coordinate system of a unit cell.*

Two coordinate systems will be used. The global (x_1,x_2) coordinate system refers to the unit cell, as illustrated in Figure 1. A local coordinate system is introduced at each grain boundary with ξ_1- and ξ_2-directions perpendicular and parallel to the grain boundary, respectively. The cell size can be characterized by $m_1 \times m_2$, where m_1 is the number of grains in the 1-direction and m_2 is the number of grains in the 2-direction. For example, the size of the unit cell in Figure 1 is $m_1 \times m_2 = 7 \times 8$.

The material in the grain is assumed to be homogeneous. In addition to the elastic deformations, the grains deform also by power law creep as a representation of ideal or secondary creep. The creep rate generally depends on stress and on temperature, but in our model the temperature is kept constant. The creep strain-rate $\dot{\epsilon}^c_{ij}$ is given by

$$\dot{\epsilon}^c_{ij} = \frac{3}{2}\,\dot{\epsilon}^c_e\,\frac{s_{ij}}{\sigma_e} \tag{1}$$

where s_{ij} is the stress deviator tensor, defined by $s_{ij} = \sigma_{ij} - \sigma_{kk}\delta_{ij}/3$, and $(\dot{})$ denotes differentiation with respect to time (summation over repeated indices implied). The effective Mises stress is defined by $\sigma_e = \sqrt{3s_{ij}s_{ij}/2}$, and $\dot{\epsilon}^c_e$ is the effective creep, which is assumed to be given by the Norton power law

$$\dot{\epsilon}_e^c = \dot{\epsilon}_0 \left(\frac{\sigma_e}{\sigma_0} \right)^n \tag{2}$$

Here, $\dot{\epsilon}_0$ is a reference strain-rate parameter, σ_0 is a reference stress parameter and n is the creep hardening exponent of the material. For a material subjected to principal stress Σ_1 and Σ_2 under plane strain, and deforming solely by power law creep according to Equations (1) and (2), the out-of-plane stress is $\Sigma_3 = (\Sigma_1 + \Sigma_2)/2$ and the corresponding effective stress is $\Sigma_e = \sqrt{3}|\Sigma_1 - \Sigma_2|/2$.

At sufficiently high temperatures, grains may slide relative to each other in a viscous manner, governed by a viscosity which is small enough to effectively relax the shear stress across grain boundaries (Ashby, 1972; Argon, 1982). In this work it is assumed that the grain boundary sliding is completely shear stress free.

Studies of the macroscopic behaviour of polycrystals with free grain boundary sliding and power law creep in grains have been carried out, for instance, by Crossman and Ashby (1975) and Ghahremani (1980). They showed that the overall creep strain-rates outnumbered the creep strain-rates with no free grain boundary sliding; i.e., free grain boundary sliding enhances the macroscopic creep strain-rate. Crossman and Ashby (1975) suggested that a polycrystal with freely sliding grain boundaries obeys an equation written in the same form as Equation (2) but with an additional stress enhancement factor f^*,

$$\dot{\epsilon}_e^c = \dot{\epsilon}_0 \left(f^* \frac{\sigma_e}{\sigma_0} \right)^n \quad (f^* > 1) \tag{3}$$

The value of f^* depends only on n and has been tabulated for planar arrays of hexagonal grains as in Figure 1 by Ghahremani (1980). Note that, strictly speaking, Equation (3) relates to the overall macroscopic response, so that $\dot{\epsilon}_e^c$ and σ_e should be interpreted as the macroscopic creep rate and effective stress, respectively. Stress and strain-rates inside grains are strongly nonuniform due to the relaxation of shear stresses on their boundary. Nevertheless, the expression (3) is expected to give a fair approximation for the relation between average creep strain-rates and stresses over a grain.

The cavities on the grain boundaries are assumed to maintain a quasi-equilibrium spherical-cap shape during growth. Let $2b$ be the spacing between cavities and a the cavity radius (see Figure 2). Then the volume of a single cavity is

$$V = \frac{4}{3} \pi a^3 h(\psi) \tag{4}$$

where $h(\psi)$ is the cavity shape parameter, defined by $h(\psi) =$

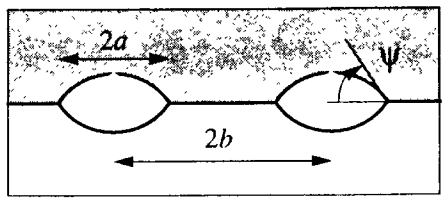

Figure 2. *Equally spaced cavities on a grain boundary.*

$[(1 + \cos\psi)^{-1} - (\cos\psi)/2]/\sin\psi$. The cavity tip angle will be taken $\psi = 75°$. Thus, the growth rate of a cavity is

$$\dot{a} = \frac{\dot{V}}{4\pi a^2 h(\psi)} \tag{5}$$

The average separation between two adjacent grains due to the presence of the grain boundary cavities is $\delta = V/(\pi b^2)$ (see Figure 3). The growth rate of the average separation is given by

$$\dot{\delta} = \frac{\dot{V}}{\pi b^2} - \frac{2V}{\pi b^2}\frac{\dot{b}}{b} \tag{6}$$

A cavity on a grain boundary grows by diffusion as well as by dislocation creep of the surrounding material. This has been studied numerically by Needleman and Rice (1980) and Sham and Needleman (1983). The following expressions approximate their results. The volumetric growth rate by diffusion is

$$\dot{V}_1 = 4\pi D \frac{\sigma_n}{\ln(1/f) - (3 - f)(1 - f)/2} \tag{7}$$

Here, σ_n is the average normal stress on the grain boundary, and D is the grain

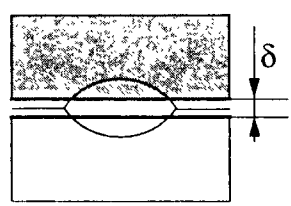

Figure 3. *The average separation between two adjacent grains due to cavities.*

boundary diffusion parameter defined by $D = D_B\delta_b\Omega/kT$, where $D_B\delta_B$ is the boundary diffusivity, Ω is the atomic volume and kT is the energy per atom measure of temperature. The parameter f in Equation (7) is determined by

$$f = \max\left\{\left(\frac{a}{b}\right)^2, \quad \left(\frac{a}{a + 1.5L}\right)^2\right\}$$

where the material parameter L, introduced by Rice (1979), is a stress and temperature dependent length scale defined by

$$L = \left(D\frac{\sigma_e}{\dot{\epsilon}_e^c}\right)^{1/3} \tag{8}$$

which accounts for the interaction between diffusion and creep. When b has a sufficiently large value, L can be seen as the length over which diffusion occurs.

For $a/L < 0.1$ approximately, the cavity growth rate by dislocation creep is negligible as compared to the growth rate by diffusion. For all cases in this report, we have used a value $a/L = 0.025$ initially, and during most of the life time a/L remains smaller than 0.1, so that the cavity growth is dominated by diffusion. Henceforth, the volumetric growth by creep is neglected, so that $\dot{V} = \dot{V}_1$. As pointed out by Dyson (1976), cavity growth and the associated separation between grains need to be accommodated by creep of the surrounding grains. For situations as stipulated above, where grain boundary diffusion is much faster than creep, diffusive cavity growth tends to become constrained by creep deformations. Consequently, load shedding away from cavitating grain facets will occur during the fracture process. Creep constrained cavity growth plays a dominant role in the growth stages of cavities; but, also during the microcrack linking-up stage creep constraint is an important concept.

To incorporate the continuous nucleation of new cavities in the present material model, we use the following cavity nucleation relation, which was proposed by Tvergaard (1985) on the basis of experimental observations of e.g. Argon (1982) and Dyson (1983):

$$\dot{N} = F_n\left(\frac{\sigma_n}{\Sigma_e}\right)^2 \dot{\epsilon}_e^c, \quad \sigma_n > 0 \tag{9}$$

In this evolution equation, N is the number of cavities per unit area on the plane of the grain boundary, and F_n is a nucleation parameter. When N reaches a saturation value N_{max} it is assumed that nucleation stops. The nucleation of new cavities of course affects the average cavity spacing. Since an area of πb^2 of the grain boundary is associated with each cavity, we may write $N = 1/(\pi b^2)$ leading to

$$\frac{\dot{b}}{b} = -\frac{1}{2}\frac{\dot{N}}{N} \tag{10}$$

Substitution of Equation (7) to Equation (9) into Equation (6) gives the average separation rate $\dot{\delta}$ in terms of the current damage state and the local stress state.

The distribution of cavities along the grain interfaces can be very nonuniform (usually causing wedge cracks), or rather homogeneous. The distribution depends on the material, on the stress level and on temperature. Ductile creep fracture typically accompanies a nonuniform distribution of cavities, while a more homogeneous distribution tends to cause brittle fracture (see, e.g., Van der Giessen and Tvergaard, 1991, 1994a). As mentioned before, we focus here on brittle fracture at elevated temperatures; accordingly, cavities are assumed to be distributed uniformly over grain boundaries. Evidently, this is only possible when also the stress is sufficiently uniform over the grain boundary. In accordance with this, the magnitudes of grain boundary quantities like a, b and σ_n that will be worked with for any grain boundary facet are averages over that facet.

When the cavities have grown to a sufficient size, coalescence will occur and an open microcrack is formed. Since the distribution of cavities over the grain interface is taken to be uniform, coalescence of all cavities on a grain boundary facet in our polycrystal model takes place when $a/b = 1$. In reality this happens only when the normal stress σ_n is very small; when the normal stress σ_n is higher, a microcrack can already occur earlier by failure of the ligament between the cavities due to ductile tearing or cleavage. Cocks and Ashby (1982) suggested that coalescence could already occur when $a/b = 0.5$. When the ratio $a/b > 0.5$, the ratio a/b grows very rapidly, even when the stresses are relatively low (e.g. Tvergaard, 1984). On the other hand, when the cavity growth process is constrained by creep, the stress on such cavitating grain boundaries will decrease so much that the stress distribution in the cell does not differ from that if those grain boundaries would have already cracked completely. Therefore, the actual critical value of a/b for coalescence has little effect on the final time to failure. Here, the value $a/b = 0.8$ is chosen as the coalescence criterion.

3. METHOD OF ANALYSIS

For the analysis of the creep failure process in polycrystalline materials, we shall make recourse to so-called Voronoi tessellations (Stoyan et al., 1985). As illustrated in Figure 4, the geometric appearance of a Voronoi tessellation and the grain structure of a polycrystalline aggregate is very similar. Assuming that grain boundary facets are flat and that grains are convex, grains may be readily identified as the polygons of a Voronoi tessellation. For the actual analysis on the basis of the constitutive relations of Section 2, it is convenient to make use of the dual representation of a Voronoi tessellation: the so-called Delaunay triangula-

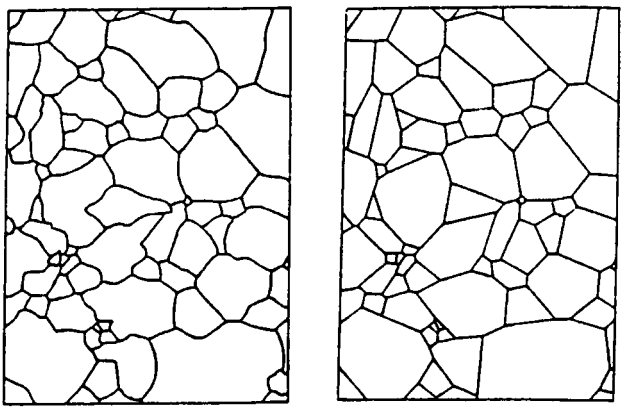

Figure 4. *(a) Polycrystalline material, (b) Voronoi tessellation.*

tion, illustrated in Figure 5. The Delaunay triangulation can be constructed in a unique way from the Voronoi tessellation, and vice versa. Each Voronoi edge, or grain boundary, is perpendicular to the corresponding Delaunay element, and situated at the middle of the element. Such representations of polycrystalline aggregates have been employed frequently in different applications; for instance, Ostoja-Starzewski and Wang (1989) used such procedures to study the effective elastic moduli of disordered materials, and Ostoja-Starzewski (1989) used it to investigate intergranular brittle cracking in random microstructures.

The use of the Delaunay network corresponding to a Voronoi tessellation in order to analyze the creep rupture process relies on the assumptions laid down

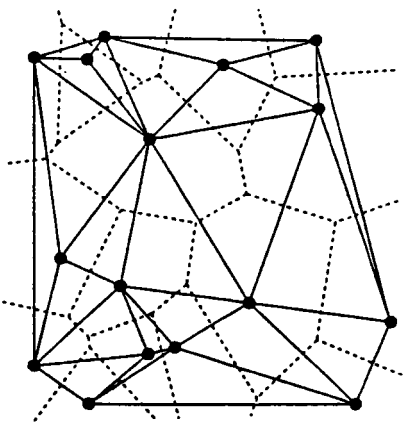

Figure 5. *Delaunay triangulation of a Voronoi tessellation.*

previously that the normal stress and cavitation state on a grain boundary facet are approximately uniform. This prompts the idea to regard each Delaunay element as a bar element corresponding to a single grain boundary facet, and to attribute to it the cavitation state in terms of a, b and δ on the facet as well as the facet normal stress. The latter is then related to the load carried by the Delaunay element, so that if this load is known at each stage of the process, the damage development in the polycrystal can be simulated in terms of the Delaunay network. Obviously, in order to be able to determine this stress state in the network, the Delaunay element will have to account also for the elastic and creep deformations in the grains adjacent to the corresponding grain boundary. Thus, a Delaunay element is a bar with special constitutive properties that should account for elastic and creep deformations of the grain material as well as for the grain boundary separation due to cavity nucleation and growth. The actual formulation of our Delaunay element for the planar polycrystal model material discussed in the previous section will now be discussed in detail.

As mentioned above, the Delaunay element that we will consider here is basically a truss or bar element whose constitutive behaviour is specified such that it behaves as much as possible conform the polycrystal model. Figure 6

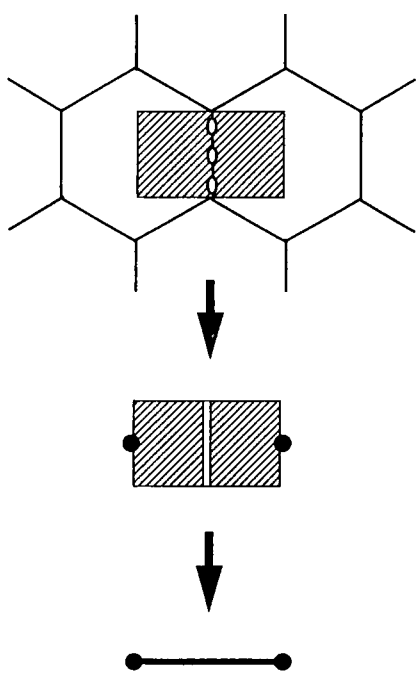

Figure 6. *Key modelling steps to a Delaunay element.*

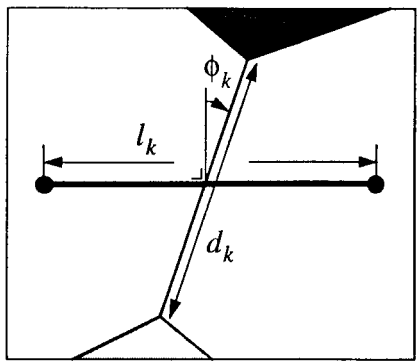

Figure 7. *Illustration of* l_k, d_k *and* ϕ_k *of element nr* k.

shows the key steps in the modelling. The Delaunay element is intended to represent a full grain boundary and parts of the adjacent grains. The Delaunay triangulation is a truss in agreement with the assumption that grains can slide freely against each other, so that the force in the bar is equal to the normal force acting on the grain boundary. In case of a regular array of hexagonal grains, the nodes of the Delaunay network coincide with the centers of the grains; when the grain shape deviates from this idealized shape, however, the nodes generally do not coincide with the centers. As discussed by Ostoja-Starzewski and Wang (1990), it is convenient to use a slightly modified Delaunay network where the nodes are taken to coincide with the centers of the grains, but where the elements cease to stand perpendicular to the grain boundary facet (see Figure 7). As a consequence, the load in the elements of such a mechanical Delaunay network introduces a shear stress on the associated boundary facet, which is in contradistinction with our assumption of free grain boundary sliding. However, if the deviations from the hexagonal shape remain sufficiently small, this fictitious shear stress is negligible, and in any case it is neglected in our modelling. Hence with Figure 7, it is seen that the normal stress σ_n on grain boundary k is obtained from the force per unit thickness σ_k (or generalized stress) in the associated kth element by

$$\sigma_n = \frac{\sigma_k \cos\phi_k}{d_k} \tag{11}$$

where d_k is the width of grain boundary k, and ϕ_k is the angle between the element normal and the grain boundary (when the element is perpendicular to the grain boundary, $\cos\phi_k = 1$).

The stress state within each grain is in general multiaxial and nonuniform, but the nonuniformity of the stress state is inherently beyond the scope of the present modelling, as mentioned already before. Assuming uniformity within each grain,

the multiaxial stress state in each grain is determined by the generalized stress in the Delaunay elements associated with its grain boundary facets; Ostoja-Starzewski (1987, 1989) discusses a procedure to actually compute the stress state. Although such a procedure would fit in the present modelling, it has an important drawback, namely that the creep deformations in each Delaunay element not only depend on its own generalized stress but also on that in all adjacent elements. In order to circumvent this, we simply assume that the stress state in that part of the grain associated with the Delaunay element under consideration (see Figure 6) is uniaxial and immediately determined from the generalized stress in the element. So, with reference to Figure 7, the grain stress σ in the grain associated with element k is taken to be given by

$$\sigma = \frac{\sigma_k}{d_k \cos\phi_k} \tag{12}$$

Note that in the absence of any cavitation, this approach introduces a physically unrealistic feature: when the applied stress Σ_1 equals Σ_2, the grain material in a Delaunay element will creep, although this applied stress state corresponds to a pure hydrostatic stress and creep should not occur. However, for the present purposes and in view of the range of creep deformations under consideration (see Section 2), the grain boundary behaviour is most important for the intergranular fracture process, and we will accept this error in the creep modelling; to get some insight into the approximations involved, we shall present a comparison with detailed full field solutions by Van der Giessen and Tvergaard (1994a, 1994b) in Section 4.1.

The generalized deformation of a Delaunay element is its elongation. This elongation is caused by elastic deformation and creep of the adjacent grains, and by the nucleation and growth of cavities on the grain boundary. With the general relations (1) to (10), the elongation of a Delaunay element can be expressed in terms of its loading, geometry and damage conditions on the grain boundary.

Recalling that the polycrystal is taken to be loaded in plain strain, the elastic elongation Δl_k^e of a Delaunay element (see Figure 7) is given by

$$\Delta l_k^e = \frac{l_k}{d_k \cos\phi_k}\left(\frac{1 - \nu^2}{E}\right)\sigma_k \tag{13}$$

where l_k is the length of the element, E is Young's modulus and ν is Poisson's ratio. With the decomposition $\Delta l_k = \Delta l_k^e + \Delta l_k^i$ of the total elongation into elastic and inelastic parts, relation (13) is rewritten in the convenient rate form

$$\dot{\sigma}_k = S_k(\dot{\Delta} l_k - \dot{\Delta} l_k^i), \quad S_k = \frac{E\, d_k \cos\phi_k}{(1 - \nu^2) l_k} \tag{14}$$

From the moment on that the grain boundary is microcracked, it cannot transmit any load. This is realized by putting the stiffness of the Delaunay element S_k to zero.

With the relations (1) and (3), it is easily seen that the elongation rate of the element by power law creep $\dot{\Delta}l_k^{cr}$ under plane strain uniaxial stress σ is given by

$$\dot{\Delta}l_k^{cr} = l_k\left(\frac{1}{2}\sqrt{3}\right)^{n+1}\dot{\epsilon}_0\left(f^*g^*\frac{|\sigma|}{\sigma_0}\right)^n\left(\frac{|\sigma|}{\sigma}\right) \tag{15}$$

Evidently, even in the absence of cavitation, the tensile stress σ differs from the macroscopic stress due to free grain boundary sliding. In the Delaunay network model, this difference is determined purely by the grain boundary facet dimensions. In order to get the proper macroscopic creep strain-rates, a geometrical factor g^* is introduced such that $g^*\,\sigma$ approximates the effective stress inside a grain, σ_e, to be substituted into Equation (3).

The elongation rate of the element due to cavity growth and nucleation in the grain boundary is determined by the average rate of separation $\dot{\delta}$ between adjacent grains,

$$\dot{\Delta}l_k^{cav} = \dot{\delta} \tag{16}$$

according to Equation (6). The effective stress to be used in (8) is approximated by $\sigma_e = \sqrt{3}|\sigma|/2$, corresponding to plane-strain uniaxial creep. The total inelastic rate of elongation of Delaunay element k is the sum of the contributions by creep and by cavitation along the axis of the element, i.e.

$$\dot{\Delta}l_k^i = \dot{\Delta}l_k^{cr} + \dot{\Delta}l_k^{cav}\cos\phi_k \tag{17}$$

here proper account has to be taken when the grain boundary coincides with a unit cell boundary.

The time evolution is solved by an explicit linear incremental method, using time steps Δt. The increment Δq of a quantity q during the time step is $\Delta q = \dot{q}\Delta t$, and is subsequently used to update the value at the end of the time step by $q(t + \Delta t) = q(t) + \Delta q$. However, to improve the numerical stability, a forward gradient scheme originally proposed by Pierce et al. (1984) is applied for integration of the constitutive equations for the inelastic elongation rate. This scheme was applied to power law creep by Tvergaard (1984) and to the grain boundary cavity growth relations by Van der Giessen and Tvergaard (1991). The idea is to introduce into the constitutive equation an estimated strain-rate as a linear interpolation between the values at time t and $t + \Delta t$: $\dot{\Delta}l_k^i = (1 - \theta) \times \dot{\Delta}l_k^{i(t)} + \theta\dot{\Delta}l_k^{i(t+\Delta t)}$. With the observation that $\dot{\Delta}l_k^i$ is governed predominantly by the stress σ_k, we then apply a Taylor series expansion to estimate $\dot{\Delta}l_k^{i(t+\Delta t)}$ as $\dot{\Delta}l_k^{i(t+\Delta t)} = \dot{\Delta}l_k^{i(t)} + (\partial\dot{\Delta}l_k^i/\partial\sigma_k)\dot{\sigma}_k\Delta t$. Combining both expressions leads to

$$\dot{\Delta}l_k^i = \dot{\Delta}l_k^{i(t)} + \theta\frac{\partial\dot{\Delta}l_k^i}{\partial\sigma_k}\dot{\sigma}_k\Delta t \tag{18}$$

which is to be substituted into the constitutive Equation (14). Written out for a single Delaunay element, we get

$$\dot{\sigma}_k = S_k^* (\dot{\Delta l}_k - \dot{\Delta l}_k^i), \text{ where } S_k^* = \frac{S_k}{1 + S_k \dfrac{\partial \dot{\Delta l}_k^i}{\partial \sigma_k} \Delta t\, \theta} \tag{19}$$

Note that the improved stiffness S_k^* is dependent on θ and the time step Δt. All computations in this report are carried out with a value of $\theta = 0.9$.

Because of symmetry, the edges of a unit cell have to remain straight throughout the process. As a consequence of cavitation and possibly microcracking, the stresses along the cell edges will be nonuniform and will vary in time. Since we want to consider cases where the applied macroscopic stresses are constant in time, the average normal stress on each of the cell edges must remain constant. This is accomplished by applying uniform displacement rate boundary conditions in the direction normal to the cell edges, while zero tractions are prescribed tangential to the cell edges. The value of the boundary velocities is determined by a Rayleigh-Ritz procedure, which is discussed in detail in the Appendix.

Due to variation in cavitation rates or the development of cracks, and the accompanying stress redistributions, some facets may become subjected to compressive stress. The cavities there can be sinter closed. For numerical convenience, cavities are considered to have closed completely when they have reached a minimum size a_m which is taken here as a constant small value.

As mentioned before, grain boundary facets that are perpendicular to the macroscopic principal tensile stress are the most prone to cavitation. Therefore, microcracks will develop most rapidly on such transverse facets. As pointed out by Rice (1981), a planar array of freely sliding grains as shown in Figure 1 immediately falls apart when all transverse facets have microcracked. In fact, failure does not need to await such a damage state but only requires a "string" of transverse microcracks running through the unit cell, such that the material on either sides of this percolation immediately separates due to the free sliding. Notice, however, that not every percolation of transverse microcracks satisfies this condition of sliding off.

4. RESULTS

The power of the Delaunay network-type modelling is its simplicity and compactness. Compared to the much more detailed analyses carried out very recently by Van der Giessen and Tvergaard (1994a, 1994b), very large unit cells can be simulated with reasonably small demands on computing time. Cells containing up to 1200 grains have been analyzed, each run requiring up to about 4 CPU hours on a Sparc station 1. Many studies may be performed within a reasonably small amount of time, but here, we shall report results for some selected cases, mainly to illustrate the accuracy of the Delaunay network model and to demon-

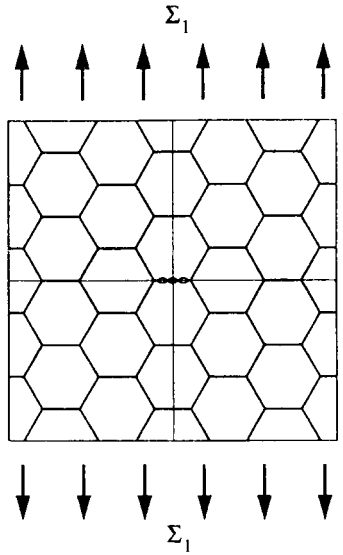

Figure 8. *Quarter of unit cell with only one cavitating facet, analyzed to compare creep results with the detailed FE model of Van der Giessen en Tvergaard (1994a).*

strate the potential capabilities of this kind of model to study various aspects of creep rupture.

In this section, we present some results for the simulated damage evolution within unit cells up consisting of regular hexagonal grains, the most simple representation of a planar polycrystal. It is noted that in this case all Delaunay elements are perpendicular to their grain boundaries, so that no spurious shear stresses are present. Within the unit cell we assume that there are two axes of symmetry concerning both geometry and material properties (e.g., see Figure 8), so that only a quarter of the unit cell has to be analyzed. In principle, any grain boundary facet may cavitate in the course of the process, but some are allowed to cavitate faster than others.

All cases to be presented are analyzed with the following material parameters. The creep exponent $n = 5$, the reference creep stress parameter $\sigma_0/E = 1.0 \times 10^{-3}$ and Poisson's ratio $\nu = 0.33$. For the time scale of the creep process, a reference time t_r is used, defined by $t_r = \Sigma_e/(E\dot{\epsilon}_e^c)$, where Σ_e is the macroscopic effective stress and $\dot{\epsilon}_e^c$ is the associated creep strain-rate according to (2). Although the stress states considered may be different, the macroscopic effective stress in all cases to be presented has the same value, $\Sigma_e/E = 0.5 \times 10^{-3}$, so that the reference times for all cases are identical. The diffusion parameter D is determined so that the length parameter L based on the macroscopic creep strain rates is given by $(a/L)_I = 0.025$ relative to the initial

cavity radius a_I; this value ensures that cavity growth is dominated by diffusion. The minimum cavity size a_m to be used in compressive regions, is taken to be 10^{-2} a_I. Various values of the nucleation parameter F_n will be considered, ranging from $F_n = 0$ (no nucleation) to $F_n = 10^3 N_I$, where N_I is the initial density $N_I = 1/(\pi b_I^2)$. The initial cavity density can also be specified by the ratio of the initial spacing b_I to the half-width $R = d/2$ of a grain boundary facet.

There are two more parameters in the model associated with creep that need to be specified, f^* and g^*. Concerning the parameter g^*, consider a hexagonal array of freely sliding hexagonal grains without any cavitation, subjected to uniaxial tension ($\Sigma_2 = 0$). It is immediately concluded from equilibrium considerations that on the transverse grain boundary facets the normal stress $\sigma_n = 1.5\Sigma_I$ (cf. Rice, 1981). Based on this observation, we take for the geometrical factor g^* in (15) a value $g^* = 1/1.5$, so that the macroscopic creep strain-rate is in accordance with Equation (3). The stress enhancement factor f^* in Equation (3) is in principle found from the analyses by Ghahremani (1980), giving $f^* = 1.19$ for $n = 5$. However, we shall not use exactly this value but, rather fine-turn its value in Section 4.1 to get optimal agreement with known accurate solutions for cavity growth in polycrystals with free sliding.

Subsequently, in Sections 4.2 and 4.3, we present some results for large cells with various microstructures in terms of distributions of nucleation rates over the grain boundary facets.

4.1 Calibration and Comparison with Full Field Solutions

To determine an adequate value for f^* for the present Delaunay model, we compare results of our analysis of a unit cell for various values of f^* with a detailed, full field analysis by van der Giessen and Tvergaard (1992) for a 5×6 unit cell subjected to uniaxial tension with $\Sigma_1/E = (1/\sqrt{3}) \times 10^{-3}$ (and $\Sigma_2 = 0$). Since creep constrained cavity growth is expected to play a central role in our failure computations for $(a/L)_I = 0.025$, we calibrate f^* for a case where cavity growth is inevitably constrained by creep: only the central grain boundary of the unit cell is taken to have cavity growth, as shown in Figure 8. On the central grain boundary, the initial cavity radius is taken to be $(a/b)_I = 0.1$, while the density is specified as b_I/R, and there is no nucleation of new cavities ($F_n = 0$). The results of the evolution of the ratio a/b on the central grain boundary facet for different values of f^* are presented in Figure 9. Also shown is the damage evolution at the center of that facet obtained from an analysis with the detailed model of Van der Giessen and Tvergaard (1994a). We note here that they found that damage was indeed practically uniform over the facet, thus confirming the presumption made in the present model. For $f^* = 1.4$ we obtain the best overall agreement of the damage evolution in comparison with the detailed analysis, so we have chosen this value to be used for further analysis.

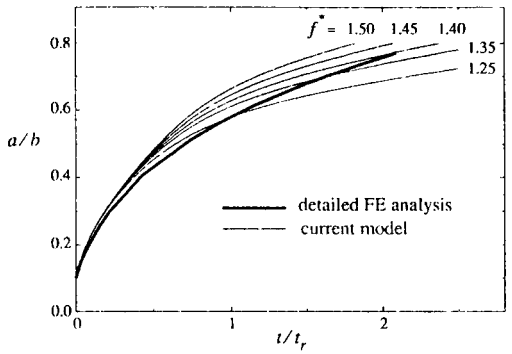

Figure 9. *Comparison of the simulations for various values of f* with detailed FE analysis.*

Clearly, the Delaunay network model involves various approximations, many of which relate to the assumption that creep deformations are slow as compared to the boundary diffusion. The latter conditions are met by the values of the material parameters mentioned above, but the final error in the computed times to failure are not easily established. In order to gain some insight in the accuracy that is obtained with the present model, we compare our results for a 5×6 unit cell subjected to uniaxial tension $\Sigma_1/E = (1/\sqrt{3}) \times 10^{-3}$ with a detailed analysis of the same problem given by Van der Giessen and Tvergaard (1994b). The particular problem is one where initially there is a microcrack at the central facet of the unit cell, while all other grain boundaries have only a low initial cavity density, specified by $b_I/R = 1$, with cavities being very small, $(a/b)_I = 0.01$. Cavity nucleation is taken to be governed by $F_n = 100N_I$. The time to failure according to the detailed analysis $t/t_r = 11.3$, while the present analysis gives $t/t_r = 10.3$.

It should be mentioned here, though, that the accuracy of the predicted times to failure is rather sensitive to the applied macroscopic stress state. As mentioned before, the Delaunay network model suffers from a spurious dependence of overall creep rates on the macroscopic stress triaxiality. Since cavity nucleation and growth will in general be constrained by creep deformations, the rate of damage accumulation will also be affected by the applied triaxiality. Henceforth, for stress states other than uniaxial tension, the ultimate times to failure are not expected to be very accurate; the process of microcracking and microcrack linking-up, however, can be described quite adequately in comparison with Van der Giessen and Tvergaard (1994b), as will be demonstrated in the next sections.

4.2 Failure Development from an Initial Imperfection

As an illustration of the potential of the Delaunay network modelling, we consider a much larger cell with $m_1 \times m_2 = 21 \times 22$. On all grain boundaries

continuous cavity nucleation is accounted for at a rate governed by $F_n = 100N_t$, except for the central grain boundary of the unit cell, which has a ten times higher nucleation activity, $F_n = 1000N_t$. The initial damage ratio is $(a/b)_t = 0.01$ while $b_t/R = 1$. The unit cell is subjected here to a biaxial stress state: $\Sigma_1/E = (2/\sqrt{3}) \times 10^{-3}$ and $\Sigma_2/\Sigma_1 = 0.5$. Figure 10 shows the Voronoi tessellation and the Delaunay triangulation of the quarter unit cell, with the central grain boundary in the lower left-hand corner. As expected, damage develops most rapidly on the central grain boundary perpendicular to the largest macroscopic principal stress; a microcrack appears at $t/t_r = 0.45$. Due to this rapid damage process, a redistribution of stress inside the unit cell occurs, so as to accelerate cavitation on some other facets. It appears that the increased stress levels tends to concentrate in a band emanating from the microcracked facet and inclined with the x_2-plane normal to the macroscopic principal stress.

The evolution of damage in the aggregate at different stages is visualized in Figure 11 by drawing the grain boundary facet with a line style dependent on the current value of the damage parameter a/b. The distribution of damage at $t/t_r = 0.6$ is shown in Figure 11(b). It is seen that the zone of higher stresses penetrates into the neighbouring unit cell, and of course vice versa. In Figure 11(b),

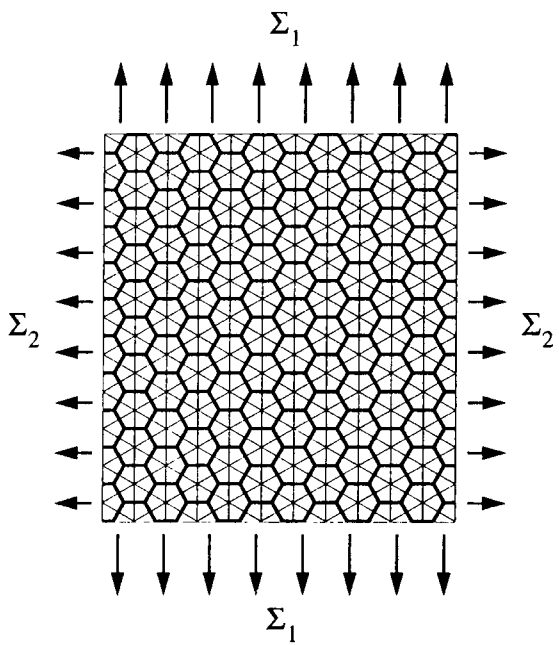

Figure 10. *Voronoi tessellation and Delaunay triangulation of geometrically regular unit cell.*

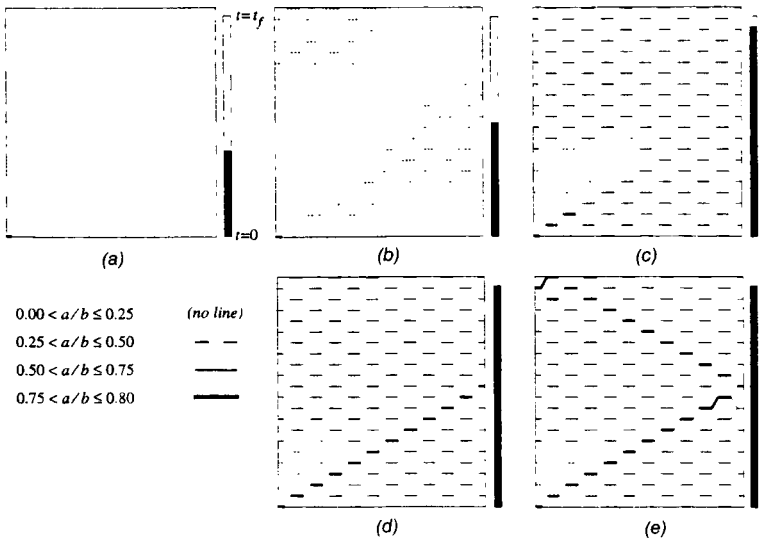

Figure 11. *The evolution of the damage parameter a/b within the quarter of a 21 × 22 unit cell with the central grain boundary having a higher nucleation activity. In (a) at* $t/t_r = 0.45$ *this facet has microcracked. Progressive failure development is shown in (b)* $t/t_r = 0.60$, *(c)* $t/t_r = 1.11$, *and (d)* $t/t_r = 1.159$ *with final failure of the aggregate in (e)* $t/t_r = 1.161$.

the stress zones of four unit cells come together in the upper left-hand corner. Inside the stress zone, grain boundaries cavitate faster than outside. Since the associated inelastic deformations have to be accommodated by the surrounding grains, the enhanced cavitation in these zones then tend to constrain cavitation in the regions between them. Thus, microcracking gives rise to a shielding effect in a rather wide zone above and below the microcrack.

The second grain boundary that microcracks is the transverse facet adjacent to the central microcrack. Within a time span of only $t/t_r = 0.01$, the next microcrack appears on the neighbouring transverse facet [see Figure 11(c)]. Now the three cracked grain boundaries in the quarter unit cell nearly double the stress on the grain boundary next to the crack front, where due to the strongly nonlinear constitutive relations, cavitation progresses so quickly that coalescence occurs almost instantaneously. At the resulting facet stress levels (exceeding $3\Sigma_1$), the cavitation strain-rates outnumber the creep strain-rates, so that the relaxation of the stress peak in front of the crack pattern will almost completely come from cavitation. By the time the stress peak due to previously cracked grain boundaries is relaxed, the facet itself has already cracked. Thus, microcrack propagation appears to be unstable and proceeds to a complete percolation almost instantaneously [see Figure 11(d)]. It is no surprise that the final crack pattern more or less follows the afore-mentioned stress zone, so that failure in this periodic array

of unit cells occurs along directions that are not perpendicular to the macroscopic principal stress but that are inclined to that at an angle of about 30°.

As mentioned before, due to the periodic boundary conditions, a percolation of transverse microcracks does not necessarily coincide with loss of integrity of the Delaunay network. Indeed, Figure 11(e) depicts a stage at a fraction of time later, showing the entrance of the microcrack pattern of the neighbouring unit cell. Looking at the polycrystalline aggregate, we now observe an "X cross weave" pattern of microcracks. It is of importance to recognize though that the crack pattern does not follow the diagonal path between neighbouring first microcracks, as illustrated in Figure 12. Final failure of the Delaunay network occurred at $t/t_r = 1.16$ as all grain boundary facets of the grain located in the top left-hand corner of the quarter unit cell microcracked [see Figure 11(e)]. Although their analyses reveal many more details of the failure process, the pattern of microcracks leading to failure are quite similar to those found by Van der Giessen and Tvergaard (1994b).

The cumulative failure time for grain boundary facets is plotted in Figure 13. The form of the curve is typical for this type of cases, showing the rapid acceleration of the failure process once two microcracks have appeared in a quarter cell We have analyzed similar cases with other unit cell sizes but keeping the aspect ratio of the cell close to unity; the material properties and initial conditions were

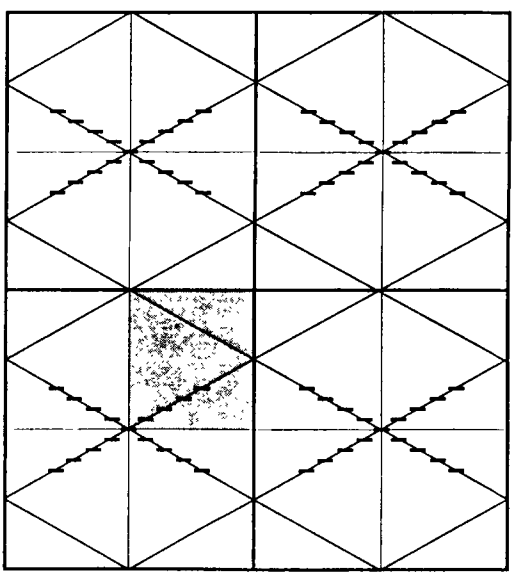

Figure 12. *X-shaped patterns of microcracks developing from central cavitating microcracks. The crack pattern does not follow the diagonal path between neighbouring first microcracks.*

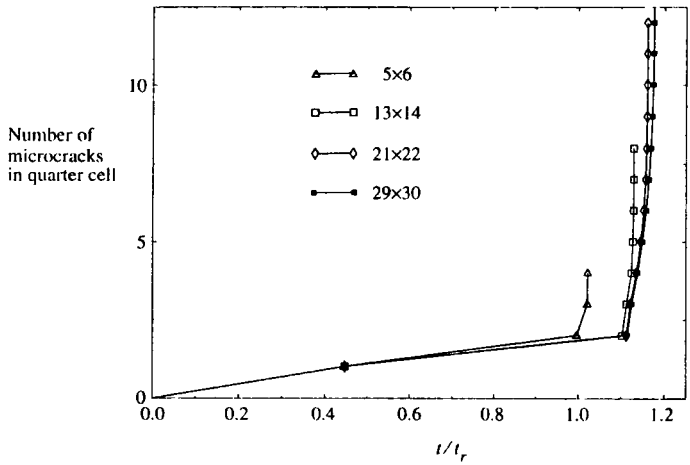

Figure 13. *Number of microcracks in time within a quarter unit cell with the central grain boundary having a higher nucleation activity (see Figure 11).*

identical. The development of damage in time was nearly equal for most cell sizes, and also the crack patterns were similar to those shown in Figure 11. For a few selected cases, the cumulative failure results are included in Figure 13. Only when the cell size became relatively small, we found that the quantitative results changed slightly. For instance, in a unit cell of size 5 × 6, the central grain boundary facet cracked at the same time as in the case of Figure 11, but the second facet microcracked somewhat earlier, at $t/t_r = 1.00$. The reason for this is that these first microcracks are now close enough to interact with each other, so as to further enhance the stresses on the remaining facets, leading to a somewhat faster damage development (cf. Van der Giessen and Tvergaard, 1994a).

4.3 Effect of Clustering

The next case analyzed is for a unit cell with the same 21 × 22 size as before, but now containing a row of five grain boundaries having the high nucleation activity, $F_n = 1000N_I$, positioned horizontally to the left and to the right of the central grain boundary facet. On all other facets the nucleation rate $F_n = 100N_I$ and the initial damage ratio $(a/b)_I = 0.01$. Also the applied stress state is identical to that for the case shown in Figure 11, $\Sigma_1/E = (2/\sqrt{3}) \times 10^{-3}$ and $\Sigma_2/\Sigma_1 = 0.5$. Because of symmetry, again only a quarter of the unit cell is simulated. The instant of microcracking at the five facets with the higher nucleation activity is nearly the same. As shown in Figure 14(a), the first microcrack to form in the quarter cell is at the outer grain boundary at $t/t_r = 0.45$ and the central grain

boundary facet is the last of the five to fail. It is seen that similar X-shaped stress zones as found previously are generated subsequently around each of the five microcracks. Near the intersection of these zones, the stresses on transverse grain boundaries is elevated, resulting in enhanced cavitation, which is also seen in Figure 14(a). The next stage shown, Figure 14(b), reveals a substantial shielding effect. Above the microcracks there is little damage accumulation, while also on the upper and lower right-hand side corners, damage evolution is somewhat slower. Note that it is not possible for the central crack to initiate an X-shaped stress zone all across the cell because of the neighbouring microcracks. The next grain boundary where cavity coalescence takes place is the left facet in the quarter unit cell of Figure 14(a) that is slightly cavitated, at $t/t_r = 0.83$, followed by the facet to the right of it at $t/t_r = 0.85$. From this situation on, the highest stress are to the right side of the microcracks making an angle with the 2-direction stress. In the unit cell two V-shaped zones of higher stress emerge now. Further microcracking now proceeds in much the same way as in the former case, as seen in Figure 14(c). This figure also shows that where the stress zones of two adjacent

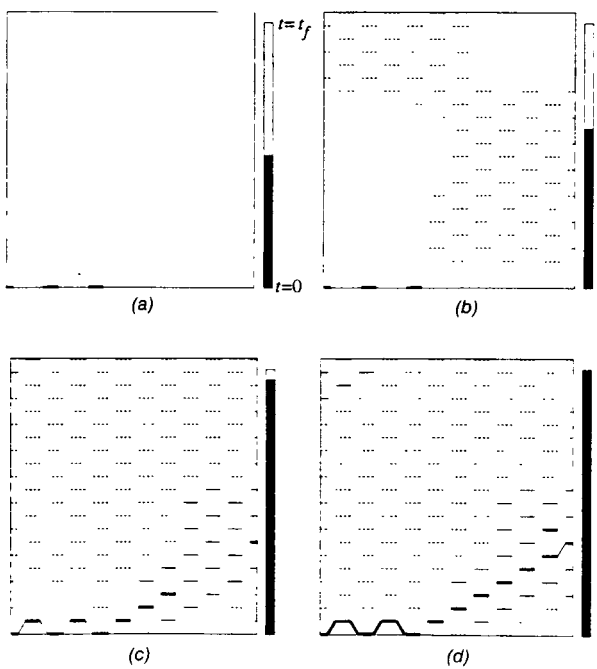

Figure 14. *The evolution of the damage parameter a/b within the quarter of a 21 × 22 unit cell containing five grain boundaries having a higher nucleation activity. (a)* $t/t_r = 0.50$; *(b)* $t/t_r = 0.60$; *(c)* $t/t_r = 0.96$; *(d)* $t/t_r = 0.97$.

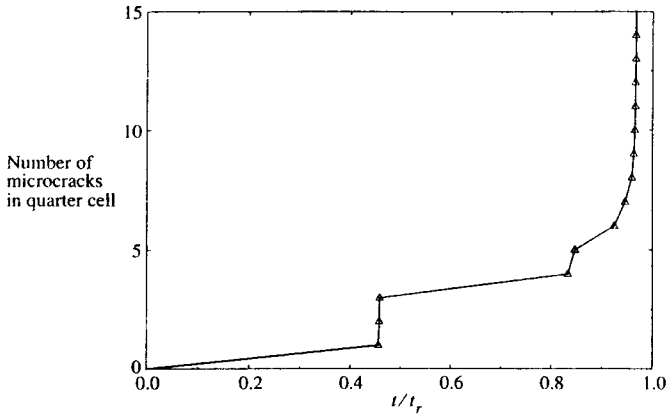

Figure 15. *Number of microcracks in time within a quarter of a unit cell containing five grain boundaries having a higher nucleation activity (see Figure 14).*

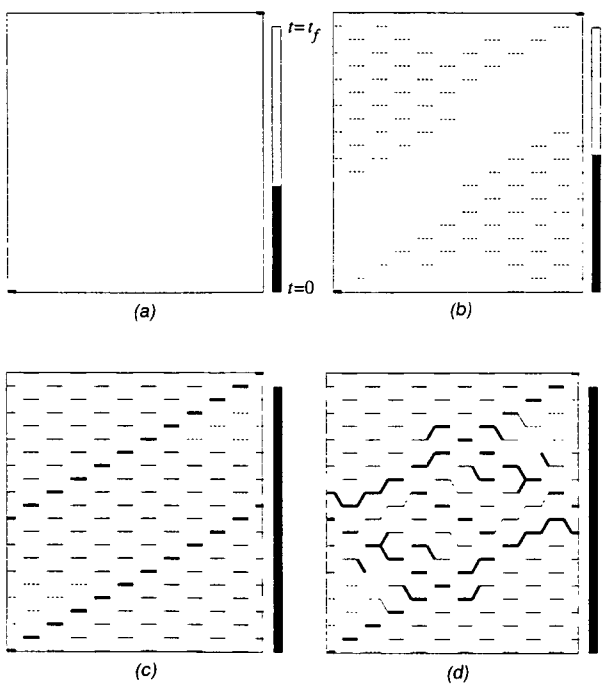

Figure 16. *The evolution of the damage parameter a/b within the quarter of a 21 × 22 unit cell with two grain boundaries having a higher nucleation activity. (a)* $t/t_r = 0.46$*; (b)* $t/t_r = 0.60$*; (c)* $t/t_r = 1.156$*; (d)* $t/t_r = 1.156$*.*

unit cells intersect, cavitation is accelerated and microcracks appear there even though they are not in the direct front of the crack pattern. As a consequence, load shedding towards the central region of the unit cell takes place, where now the grain boundary facets that are inclined to the maximum principal stress direction are cavitating until microcracking also occurs there. The simulation stopped as all grain facets of the grain in the left-hand bottom corner in Figure 14(d) failed. A cumulative plot of the number of microcracks versus time is depicted in Figure 15. The end of the curve is again nearly vertical, but the transition is much less abrupt than in Figure 13.

The last analysis presented here is for the same size of the unit cell, 21 × 22, but contains two grain boundaries with the 10 times higher nucleation activity, $F_n = 1000N_l$. One of the faster nucleating facets is the central grain boundary and the other is at top righthand side corner of the unit cell. The applied stress state, material properties and the initial cavitation state on all other facets is the same as in the previous cases. The development of the damage evolution is nearly the same as in the unit cell with only one central fast cavitating facet. Here, both fastly nucleating facets microcrack at $t/t_r = 0.46$ as can be seen in Figure 16(a). The accompanying stress redistribution for each of the microcracks, shown in Figure 16(b), is similar to that in Figure 11(b), but of course now there are two stress zones. This results in a similar crack pattern [see Figure 16(c)]. Further microcracking until failure, depicted in Figure 16(d), took place in a relatively short period of time of about $t/t_r = 0.001$.

5. DISCUSSION AND CONCLUSION

A Delaunay network model has been presented for the analysis of creep failure in planar polycrystal models due to the nucleation and growth of grain boundary cavities. The model is based on a representation of a polycrystal which is dual to the intuitive Voronoi representation, where Delaunay elements represent individual grain boundary facets along with parts of the creeping grains on either side of the facet. Assuming stress free grain boundary sliding, a polycrystal is essentially modelled as a truss structure, with the Delaunay elements serving as truss elements with a special nonlinear constitutive behaviour which is governed by cavitation and creep. The formulation applies to problems which involve brittle type creep failure.

The network representation allows large polycrystalline aggregates to be analyzed with rather mild computational requirements. This kind of modelling seems to be particularly suited to study the development of failure through the formation of microcracks and the subsequent linking-up of microcracks. Despite the approximations involved, comparison with full field analyses of milar unit cell problems (Van der Giessen and Tvergaard, 1994a, 1994b) shows that microcrack patterns are predicted with fair agreement. The predicted failure times also seem to agree reasonably well for applied stress states of low stress triaxiality.

For increasing triaxiality, the predictions loose their quantitative accuracy due to the fact that creep of the grains is not represented adequately under such circumstances.

Illustrative examples of unit cell analyses have demonstrated the continuous redistribution of grain boundary stresses within the polycrystal due to creep constrained cavitation during particularly the early stages of the process and due to microcrack propagation at later stages. In agreement with experimental observations, grain boundary facets normal to the maximum principal tensile stress direction tend to fail first, but the macroscopic crack path in a unit cell does not necessarily show a tendency to propagate perpendicular to that direction too. Rather, propagation is seen to take place in all cases shown here along a direction that is inclined with that direction, similar to what has been found by Van der Giessen and Tvergaard (1994b). Results for relatively large unit cells show that the time to failure is considerably larger than the time to form the first microcrack, and they also demonstrate the acceleration of creep damage evolution as soon as a few grain boundary facets in the cell have microcracked.

In this paper, the examples have focused on regular polycrystals with hexagonal grains and uniform material properties, except for a few individual facets with a higher nucleation activity which serve as initial imperfections. However, this Delaunay network modelling seems to be particularly suited to study failure in polycrystals with more random grain sizes and grain shapes, as well as random variations of material properties over the grain boundary facets. A more systematic study of such aspects will be reported elsewhere. It is also noted that, in principle, the network modelling is readily extended to 3-D polycrystals.

It is tempting to relate the Delaunay network modelling of polycrystals here with the so-called lattice models that have recently found application in different areas of physics [see, e.g., Herrmann and Roux (1990) for a review]. In particular, lattice models have been used with remarkable success to model the fracture behaviour in brittle materials like concrete (e.g. Bazant et al., 1990; Schlangen and van Mier, 1992), polymers (e.g. Termonia et al., 1990) and other materials (e.g. Ostoja-Starzewski and Wang, 1989; Duxbury and Kim, 1990). Although the precise identification of the elements of the networks differs, there are, in general, two key differences with the present modelling. First of all, in many applications of lattice models, there is only a weak relationship between the lattice structure and the actual microstructure of the material under consideration. In most cases, a lattice of beam elements is used merely to represent the mechanical response of the material, that for all other purposes is regarded as a continuous but inhomogeneous medium. In the present model, Delaunay elements directly correspond to grain boundary facets which, for the failure mechanism under consideration here, form the relevant microstructure. Hence, failure of a Delaunay element represents actual failure sites, while failure of an element in the lattice modelling in the above references usually cannot be identified with any entity in

the microstructure. The second difference regards the modelling of the failure mechanism itself. Most lattice models use simple loading criteria to signal failure of the lattice beams. Here, however, we intend to follow the entire damage evolution up to failure by coalescence of voids on the basis of well-identified physically based models. As a consequence, all parameters in the present network model have a direct physical interpretation (although some parameters like diffusion coefficients can only be measured with limited accuracy), whereas the material parameters governng failure in lattice models often are of a purely phenomenological nature. Those two reasons give us reason to regard the present network modelling as quite distinct from most lattice models.

ACKNOWLEDGEMENTS

The research of Marc van der Burg was made possible by Shell Research, Arnhem, The Netherlands. We want to thank Geert Stam and Jan Booy for their continuous computational support.

APPENDIX

In this appendix, the Rayleigh-Ritz procedure is described, which is used to determine the boundary displacement increments in accordance with the macroscopic stress state.

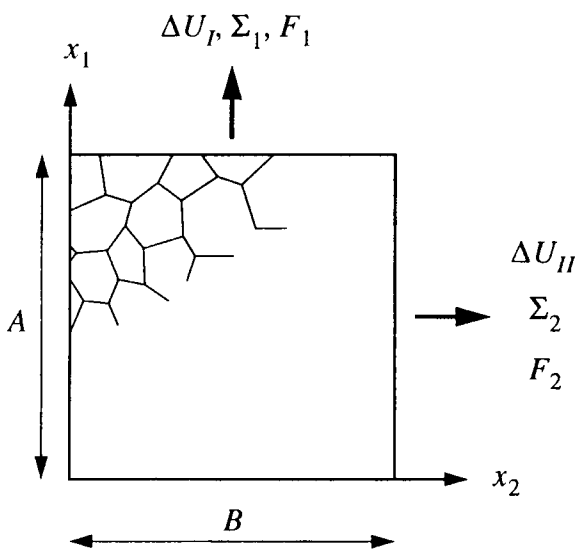

Figure 17. *Quantities used in the Rayleigh-Ritz procedure for the quarter unit cell.*

The total vector $\Delta \boldsymbol{u}$ of nodal displacement increments can be split up as

$$\Delta \boldsymbol{u} = [\Delta \boldsymbol{u}_I; \Delta \boldsymbol{u}_{II}; \Delta \boldsymbol{v}]^T \tag{A.1}$$

where the vector $\Delta \boldsymbol{u}_I$ contains the horizontal nodal displacement increments (magnitude ΔU_I) along $x_1 = A$, and the vector $\Delta \boldsymbol{u}_{II}$ contains the vertical nodal displacement increments (magnitude ΔU_{II}) along $x_2 = B$ (see also Figure 17). The vector $\Delta \boldsymbol{v}$ contains all remaining nodal displacement increments. The magnitudes ΔU_I and ΔU_{II} are unknown, and are to be determined form the conditions that the corresponding average stresses in x_1 and x_2 directions retain fixed values Σ_1 and Σ_2, respectively. We shall determine ΔU_I and ΔU_{II} using a Rayleigh-Ritz technique combined with the FE program, as proposed by Needleman and Tvergaard (1984).

The incremental FE equations are written as $\boldsymbol{K}\Delta \boldsymbol{u} = \Delta \boldsymbol{F} - \boldsymbol{B}$, where $\boldsymbol{K}$ is the global stiffness matrix. The vector $\Delta \boldsymbol{F}$ contains the external load increments, and vector $\boldsymbol{B}$ contains the equilibrium correction and the contribution $\boldsymbol{D}^T\boldsymbol{S}^*\Delta \boldsymbol{l}^i$ from inelastic deformations.

Now, perform three trial solutions:

1. a unit increment ΔU_I along $x_1 = A$:

$$\Delta \boldsymbol{u}_{(1)} = [\mathbf{1};\mathbf{0};\Delta \boldsymbol{v}_{(1)}]^T$$

$$\Delta \boldsymbol{F}_{(1)} = [\Delta \boldsymbol{F}_I^{(1)};\ \Delta \boldsymbol{F}_{II}^{(1)};\ \mathbf{0}]^T$$

$$\boldsymbol{B}_{(1)} = [\mathbf{0};\mathbf{0};\mathbf{0}]^T$$

2. a unit increment ΔU_{II} along $x_2 = B$:

$$\Delta \boldsymbol{u}_{(2)} = [\mathbf{0};\mathbf{1};\Delta \boldsymbol{v}_{(2)}]^T$$

$$\Delta \boldsymbol{F}_{(2)} = [\Delta \boldsymbol{F}_I^{(2)};\ \Delta \boldsymbol{F}_{II}^{(2)};\ \mathbf{0}]^T$$

$$\boldsymbol{B}_{(2)} = [\mathbf{0};\mathbf{0};\mathbf{0}]^T$$

3. no load increment, only the equilibrium correction and the contribution of the inelastic deformations $\boldsymbol{D}^T\boldsymbol{S}^*\ \Delta \boldsymbol{l}^i$:

$$\Delta \boldsymbol{u}_{(3)} = [\Delta \boldsymbol{u}_I^{(3)};\Delta \boldsymbol{u}_{II}^{(3)};\Delta \boldsymbol{v}_{(3)}]^T$$

$$\Delta \boldsymbol{F}_{(3)} = [\mathbf{0};\mathbf{0};\mathbf{0}]^T$$

$$\boldsymbol{B}_{(3)} = \boldsymbol{B}$$

The final actual solution can then be written as

$$\Delta \boldsymbol{u} = \sum_{i=1}^{3} \delta_i \Delta \boldsymbol{u}_{(i)} \tag{A.2}$$

where $\delta_1 \equiv \Delta U_I$, $\delta_2 \equiv \Delta U_{II}$, $\delta_3 \equiv 1$. Substituting this into (A.1),

$$\sum_{j=1}^{3} \delta_j \boldsymbol{K} \Delta \boldsymbol{u}_{(j)} = \Delta \boldsymbol{F} - \boldsymbol{B} \tag{A.3}$$

and multiplying by $\Delta \boldsymbol{u}_{(i)}^T$ gives a system of linear equations for δ_i,

$$\sum_{j=1}^{3} r_{ij} \delta_j = \Delta f_i - b_i \tag{A.4}$$

where $r_{ij} = \Delta \boldsymbol{u}_{(i)}^T \boldsymbol{K} \Delta \boldsymbol{u}_{(j)}$, $\Delta f_i = \Delta \boldsymbol{u}_{(i)}^T \Delta \boldsymbol{F}$ and $b_i = \Delta \boldsymbol{u}_{(i)}^T \boldsymbol{B}$. Partial rewriting of (A.2) gives

$$\begin{bmatrix} r_{11} & r_{12} & r_{13} \\ r_{21} & r_{22} & r_{23} \end{bmatrix} \begin{bmatrix} \Delta U_I \\ \Delta U_{II} \\ 1 \end{bmatrix} = \begin{bmatrix} \Delta F_1 \\ \Delta F_2 \end{bmatrix} - \begin{bmatrix} b_1 \\ b_2 \end{bmatrix}$$

where ΔF_1 and ΔF_2 are increments of the total forces F_1 and F_2 in x_1 and x_2 direction, respectively. The stresses Σ_1 and Σ_2 are constant, so $F_1 = \Sigma_1 B$ and $F_2 = \Sigma_2 A$ and the increments are $\Delta F_1 = \Sigma_1 \Delta B = \Sigma_2 \Delta U_{II}$ and $\Delta F_2 = \Sigma_2 \Delta A = \Sigma_2 \Delta U_I$. Substitution into (A.5) gives

$$\begin{bmatrix} r_{11} & r_{12} - \Sigma_1 \\ r_{21} - \Sigma_2 & r_{22} \end{bmatrix} \begin{bmatrix} \Delta U_I \\ \Delta U_{II} \end{bmatrix} = - \begin{bmatrix} b_1 \\ b_2 \end{bmatrix} - \begin{bmatrix} r_{13} \\ r_{23} \end{bmatrix} \tag{A.6}$$

from which the unknown ΔU_I and ΔU_{II} can be solved. With Equation (A.2), the total displacement vector $\Delta \boldsymbol{u}$ can be determined.

REFERENCES

Argon, A. S. 1982. In *Recent Advances in Creep and Fracture of Engineering Materials and Structures*, B. Wilshire and D. R. J. Owen, eds., UK: Pineridge Press, pp. 1–52.

Ashby, M. F. 1972. *Surface Science*, 31:498–542.

Bazant, Z. P., M. R. Tabarra, M. T. Kazemi and G. Pijaudier-Cabot. 1990. *ASCE Journal of Engineering Mechanics*, 116:1686–1705.

Cocks, A. C. F. and M. F. Ashby. 1982. *Progress in Materials Science*, 27:199–244.

Crossman, F. W. and M. F. Ashby. 1975. *Acta Metallurgica*, 23:425–440.

Duxbury, P. M. and S. G. Kim. 1990. In *Mechanical Properties of Porous and Cellular Materials*, K. Sieradzki, D. J. Green and L. J. Gibson, eds., Pittsburgh, PA: Materials Research Society, pp. 179–195.

Dyson, B. F. 1976. *Metal Science*, 10:349–353.

Dyson, B. F. 1983. *Scripta Metallurgica*, 17:31–37.

Ghahremani, F. 1980. *International Journal of Solids and Structures*, 16:847–862.

Herrmann, H. J. and S. Roux. 1990. *Statistical Models for the Fracture of Disordered Media*, Amsterdam: North-Holland Elzevier Science Publishers.

Hull, D. and D. E. Rimmer. 1959. *Philosophical Magazine*, 4:673–687.

Needleman, A. and J. C. Rice. 1980. *Acta Metallurgica*, 28:1315–1332.

Needleman, A. and V. Tvergaard. 1984. *Finite ELement Special Problems in Solid Mechanics, Vol. V*, J. T. Oden and G. F. Carey, eds., Prentice Hall.

Ostoja-Starzewski, M. 1987. *Mechanics Research Communications*, 14(4):255–262.

Ostoja-Starzewski, M. and C. Wang. 1989. *Acta Mechanica*, 80:61–80.

Ostoja-Starzewski, M. 1989. *Applied Mechanics Reviews*, 42:S202–S212.

Ostoja-Starzewski, M. and C. Wang. 1990. *Acta Mechanica*, 84:47–61.

Pierce, D., C. F. Shih and A. Needleman. 1984. *Computers and Structures*, 18:875–887.

Rice, J. R. 1979. *Time Dependent Fracture of Materials at Elevated Temperature*, S. Wolf., ed., Germantown, MD: U.S. Department of Energy Report CONF 790236 UC-25, p. 130.

Rice, J. R. 1981. *Acta Metallurgica*, 29:675–681.

Schlangen, E. and J. G. M. van Mier. 1992. *International Journal of Damage Mechanics, 1:435*–454.

Sham, T. L. and A. Needleman. 1983. *Acta Metallurgica*, 31:919–926.

Stoyan, D., W. S. Kendall and J. Mecke. 1985. *Stochastic Geometry and Its Applications*, New York: John Wiley & Sons.

Termonia, Y., P. Meakin and P. Smith. 1990. *Macromolecules*, 18:2246–2252.

Tvergaard, V. 1984. *Journal of the Mechanics and Physics of Solids*, 32:373–393.

Tvergaard, V. 1985. *Journal of the Mechanics and Physics of Solids*, 33:447–469.

Van der Giessen, E. and V. Tvergaard. 1991. *International Journal of Fracture*, 48:153–178.

Van der Giessen, E. and V. Tvergaard. 1994a. *Mechanics of Materials*, 17:47–69.

Van der Giessen, E. and V. Tvergaard. 1994b. *Acta Metallurgica et Materialia*, 42:959–973.